

LETTER TO THE EDITOR

A high resolution line survey of IRC +10216 with *Herschel*/HIFI[★]

First results: Detection of warm silicon dicarbide (SiC₂)

José Cernicharo¹, L.B.F.M. Waters^{2,3}, Leen Decin^{2,3}, Pierre Encrenaz⁴, A.G.G.M. Tielens⁵, Marcelino Agúndez^{1,6}, Elvire De Beck³, Holger S.P. Müller⁷, Javier R. Goicoechea¹, Michael J. Barlow⁸, Arnold Benz⁹, Nicolas Crimier¹, Fabien Daniel^{1,4}, Anna Maria Di Giorgio¹⁰, Michel Fich¹¹, Todd Gaier¹², Pedro García-Lario¹³, Alex de Koter^{2,14}, Theo Khouri², René Liseau¹⁵, Robin Lombaert³, Neal Erickson¹⁶, Juan R. Pardo¹, John C. Pearson¹², Russell Shipman¹⁷, Carmen Sánchez Contreras¹, David Teyssier¹³

(Affiliations can be found after the references)

Received / accepted

ABSTRACT

We present the first results of a high-spectral-resolution survey of the carbon-rich evolved star IRC +10216 that was carried out with the HIFI spectrometer onboard *Herschel*. This survey covers all HIFI bands, with a spectral range from 488 to 1901 GHz. In this letter we focus on the band-1b spectrum, in a spectral range 554.5 – 636.5 GHz, where we identified 130 spectral features with intensities above 0.03 K and a signal-to-noise ratio >5. Detected lines arise from HCN, SiO, SiS, CS, CO, metal-bearing species and, surprisingly, silicon dicarbide (SiC₂). We identified 55 SiC₂ transitions involving energy levels between 300 and 900 K. By analysing these rotational lines, we conclude that SiC₂ is produced in the *inner* dust formation zone, with an abundance of $\sim 2 \times 10^{-7}$ relative to molecular hydrogen. These SiC₂ lines have been observed for the first time in space and have been used to derive an SiC₂ rotational temperature of ~ 204 K and a source-averaged column density of $\sim 6.4 \times 10^{15}$ cm⁻². Furthermore, the high quality of the HIFI data set was used to improve the spectroscopic rotational constants of SiC₂.

Key words. Stars: individual: IRC +10216 — stars: carbon — astrochemistry — line:identification — stars: AGB and post-AGB

1. Introduction

Circumstellar envelopes (CSEs) of evolved stars foster a remarkably complex chemistry. The reactions behind molecular synthesis, how they vary from the inner to the outer layers of the expanding envelope, their relationship to dust grain formation, and the chemical evolution from the asymptotic giant branch (AGB) to the post AGB-phases, are all important questions that still need answers (Cernicharo, 2004; Herpin & Cernicharo, 2001; Herpin et al., 2002). Observations at different wavelength ranges are clearly required with this purpose in mind. The atmosphere and the inner dust condensation regions are best probed by infrared (IR) ro-vibrational lines or by high-*J* lines in the ground and vibrationally excited states of abundant species such as CO, HCN, and SiS (Fonfría et al., 2008; Cernicharo et al., 1996a; Decin et al., 2010; Patel et al., 2009). The outer and colder layers of the CSE are best probed by molecular rotational lines at millimeter wavelengths (Cernicharo et al., 2000; Kemper et al., 2003; Agúndez & Cernicharo, 2006; He et al., 2008). Based on a large set of high spectral resolution data, the physical conditions of the different regions of the CSE can be constrained by providing a complete picture of the object; see, e.g., Agúndez (2009); Cernicharo et al. (2000); Pardo & Cernicharo (2007); Patel et al. (2009). Of particular interest are the high angular resolution observations by Lucas et al. (1995, 1997) and Patel et al. (2009) of the innermost region of the envelope.

IRC +10216 (CW Leo) is one of the brightest infrared sources in the sky, making it an ideal target to observe with the *Herschel Space Observatory* (Pilbratt et al., 2010). Most of the molecules detected in this source are heavy carbon-chain radicals (Cernicharo & Guélin, 1996b), metal-bearing species (Cernicharo & Guélin, 1987), anions (see, e.g., McCarthy et al. (2006); Cernicharo et al. (2008) and references therein), and many diatomic and triatomic molecules. The HIFI instrument (de Graauw et al., 2010) provides both a high spectral resolution and a wide spectral coverage. The first is necessary for resolving the complex kinematics characteristic of IRC +10216, allowing us to distinguish between the contribution from the inner acceleration zone (Fonfría et al., 2008; Cernicharo et al., 2010a; Decin et al., 2010) and from the expanding envelope where the gas reaches its terminal velocity (Agúndez, 2009). The wide spectral coverage is mandatory for a complete inventory of lines to study the chemical content and molecular excitation in detail. In this *Letter* we present the preliminary results of a full line survey of IRC +10216 taken with HIFI between 480 and 1900 GHz, and highlight the range 554-636 GHz. We focus on silicon dicarbide, SiC₂ (Thaddeus et al., 1984), a triatomic molecule that, together with HCN, is the main contributor to the forest of lines observed in the submillimeter and far-infrared domains.

2. Observations and data reduction

HIFI observations (de Graauw et al., 2010) were carried out May 11-15 2010. In-orbit instrument performances are described in detail by Roelfsema et al. (2010). This survey uses all HIFI bands, providing a frequency coverage between 488

[★] *Herschel* is an ESA space observatory with science instruments provided by European-led Principal Investigator consortia and with important participation from NASA

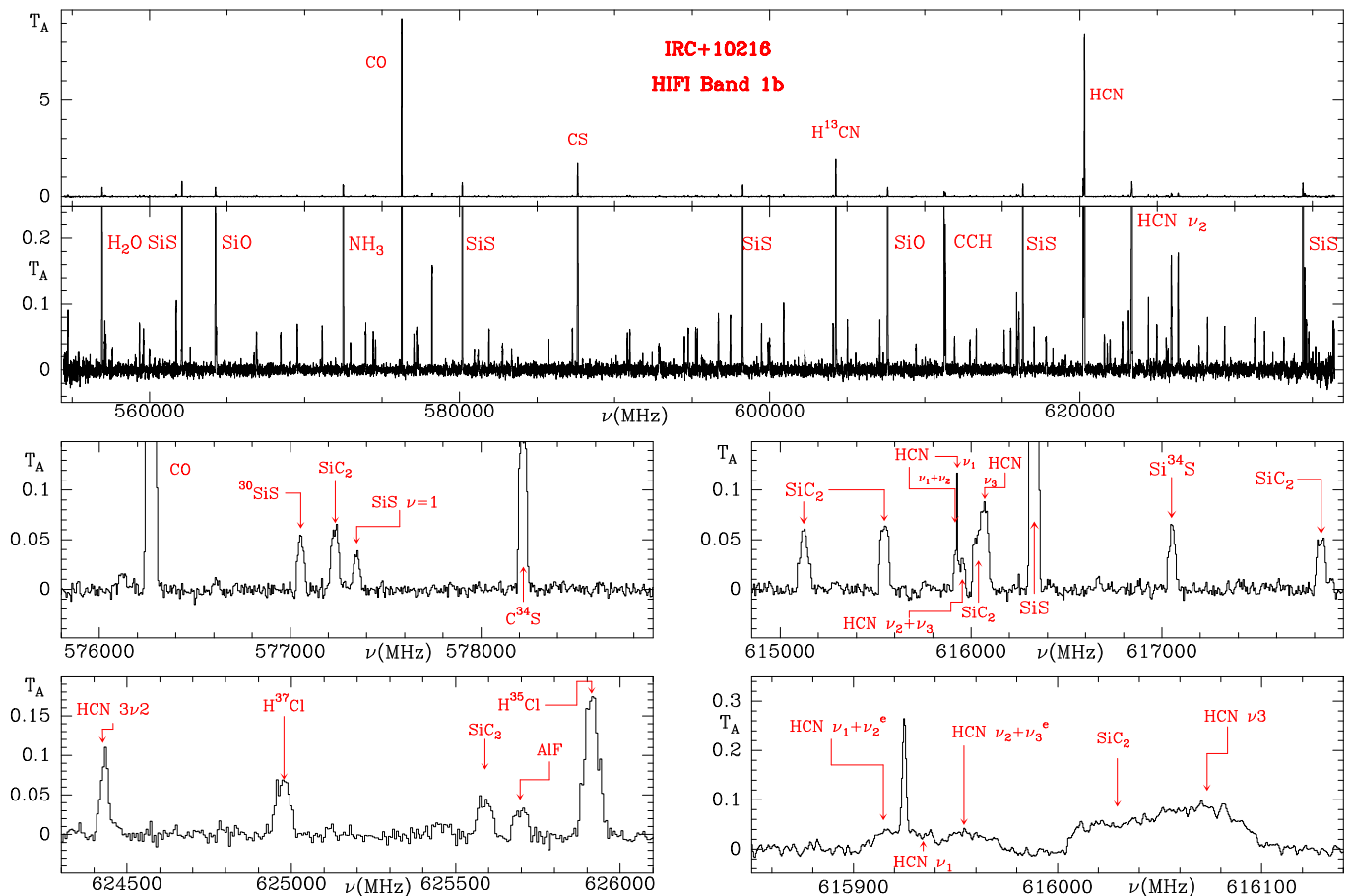


Fig. 1. Spectra of IRC +10216 observed with HIFI band 1b. The two upper panels present the complete spectrum on two different intensity scales. The panels below show different 3 GHz wide ranges of the survey. All data have been smoothed to a spectral resolution of 2.8 km s^{-1} except for the right bottom panel, which shows the spectrum around several vibrational lines of HCN with the nominal WBS resolution (1.1 MHz , $\approx 0.5 \text{ km s}^{-1}$).

and 1901 GHz. We present the spectral scan of IRC +10216 in band 1b (554.5–636.5 GHz), corresponding to the data of OBSID1342196414. The main-beam antenna efficiency at 600 GHz is 0.75 and the half-power beam width is $36''$. The data were taken in double beam-switching mode at a frequency resolution of 1.1 MHz. The total integration time per frequency setting was 30.6 seconds (ON+OFF). The measured rms noise for each individual frequency setting is between 25–40 mK depending on the frequency. Averaging all scans (see below) brings the measured rms noise down to values between 7 and 12 mK. The data were processed using the standard *Herschel* pipeline up to Level 2, providing fully calibrated spectra of the source. We then analyzed them with the GILDAS-CLASS90 software¹.

The single side band spectrum of receiver 1b was obtained through a standard manual procedure. We first removed spurious features (one) and then compared all scans one by one for a given frequency to remove unwanted lines from the corresponding image side band by blanking out the corresponding channels. In the few cases where image band lines were blended with signal band lines, a fit was performed to the blended lines to separate the contribution from each band. The image band emission was then subtracted from the signal band spectrum. This procedure was repeated twice in order to ensure a complete cleaning of lines from the image side band at each frequency setting. Once

the deconvolution was done for one of the receivers, the other receiver was treated automatically by blanking out the same frequency blocks in each individual scan. Linear baselines were subtracted and all 1456 single side band individual scans (728 per receiver) merged. The calibration and the double side band gain ratio was checked against the strongest lines, and found to be consistent within 2–4%. The final spectrum with a spectral resolution of 2.8 km s^{-1} is shown in Fig. 1.

3. Results

While ground-based observations have provided much insight into the chemical inventory, the unprecedented spectral coverage of HIFI will yield many lines arising from a wide variety of species that together will greatly expand our understanding of the density, temperature, and dynamical structure of the ejecta and the processes driving the molecular complexity of these chemical “smokestacks” of the galaxy, from the dust forming zones to the radical and photodominated outer regions. In this work we present the first high spectral resolution line survey towards an evolved star in the submillimeter and far-IR domains. Figure 1 shows around 130 well-detected lines with intensities exceeding 30 mK. All of them, except one, can be easily assigned to lines of CO (including $\nu=1$; see Patel et al. 2009b), HCN and H¹³CN (in several vibrational states), SiO, SiS, and CS (including its isotopologs and vibrationally excited levels), AIF, and AlCl. All these species have been pre-

¹ See <http://www.iram.fr/IRAMFR/GILDAS> for more information about GILDAS softwares.

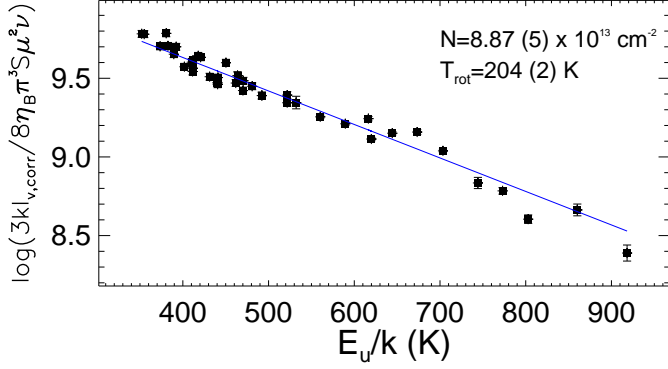


Fig. 2. Rotational diagram for the observed SiC₂ lines. The rotational temperature is 204 K and the beam averaged column density of SiC₂ is $8.9 \times 10^{13} \text{ cm}^{-2}$.

viously detected by several authors (Cernicharo et al., 2000; Cernicharo & Guélin, 1987; Turner, 1987; Lucas & Cernicharo, 1989; Lucas et al., 1995; Lucas, 1997; Fonfría et al., 2006; Patel et al., 2009). Of particular interest are the $J=1-0$ lines of HCl and H³⁷Cl, shown in the bottom left panel of Fig. 1. Cernicharo et al. (2010b) have recently detected these species towards IRC +10216 using the PACS and SPIRE instruments (Poglitsch et al., 2010; Griffin et al., 2010), and the present results definitively confirm this detection. From the HIFI data we derive $X(^{35}\text{Cl})/X(^{37}\text{Cl})=2.5 \pm 0.2$, consistent with the value derived from the metal-bearing species NaCl, AlCl, and KCl isotopologs (Cernicharo & Guélin, 1987; Cernicharo et al., 2000), and very close to the Solar System value of 3 and the one derived with HIFI in the ISM (Cernicharo et al., 2010c).

HCN is known to show maser emission in its bending mode and in high vibrationally excited states (Guilloteau et al., 1987; Lucas & Cernicharo, 1989; Schilke et al., 2000; Schilke & Menten, 2003). Except for one of the HCN $J=6-5$ lines, all HCN lines in band 1b seem to be thermal in nature. Figure 1 (right bottom panel) shows that, in addition to a pedestal of thermal emission due to $\nu_1 + \nu_2^{1e}$, $\nu_2 + \nu_3^{1e}$ and ν_1 vibrational levels, there is a clearly distinguished narrow feature that is likely a maser line. It can be assigned to ν_1 or to the $\nu_1 + \nu_2^{1e}$ vibrational level (Zelinger et al., 2003). However, without a full detailed treatment of the HCN radiative transfer, it is difficult to assign it to one or the other. The $\nu_1 + \nu_2^{1f}$ $J=6-5$ line does not show such any equivalent feature. From a very quick look at the line survey data in other HIFI bands, it appears that the number of HCN masers is quite impressive and does not have any systematic pattern within a given vibrational level. It is worth noting that the ν_1 and ν_3 $J=1-0$ lines of HCN have been observed with the IRAM 30m telescope at the level of a few mK. The HIFI data show the importance of increasingly higher frequencies (hence higher Einstein coefficients and line opacities) to observe the warm layers of CSEs. In particular, Cernicharo et al. (2010a) have found many lines of HCN $J=3-2$ from vibrational levels up to 10000 K. The $J=6-5$ lines of these vibrationally excited levels (up to 6000-7000 K) also appear in the HIFI line survey of band 1b and will be presented and analyzed in a forthcoming paper. Other species such as H₂O and NH₃ are analyzed within the HIFISTARS Guaranteed Time Key Program (Bujarrabal et al., 2010). In addition to the lines and species presented above, we clearly detect 41 spectral features that belong to 55 rotational transitions of SiC₂, of which 14 are doublets at the same frequency. SiC₂ emission reaches its

maximum at millimeter wavelengths in a shell with a radius of 15'' like the radicals C_nH (Guélin et al., 1993; Lucas et al., 1995). However, interferometric and single-dish observations of this molecule also indicate a large abundance in the inner envelope (Gensheimer et al. 1995; Lucas et al. 1995; Cernicharo et al. 2000; Agúndez 2009; Patelet al 2009). Table A.1 (see appendix A in the electronic version of the paper) provides the observed parameters for the detected SiC₂ lines. All of them arise from levels involving energies between 300-900 K and have flat-topped profiles (see Fig. 1 & 4), therefore indicating that they are formed in the inner, warm layers of the CSE. We found that the predicted frequencies for these lines were in error by several MHz so we provide a new set of rotational constants in Appendix A.

4. Discussion

The observed SiC₂ line intensities (see Table A.1) were used to determine the rotational temperature T_{rot} and the column density $N(\text{SiC}_2)$ of the emitting gas. The rotational diagram in Fig. 2 yields $T_{rot}=204 \pm 2 \text{ K}$ and $N(\text{SiC}_2)=8.9(1) \times 10^{13} \text{ cm}^{-2}$ (averaged over the beam of HIFI at 636 GHz). The relatively high rotational temperature implies that the excitation region of the considered emission lines is smaller than about 2'' in radius. This region corresponds to a kinetic temperature $T_K > 100 \text{ K}$, according to the expected T_K radial profile (see, e.g., Fonfría et al. 2008 and Fig. 3). Consequently, the source-averaged column density of SiC₂ is $6.4 \times 10^{15} \text{ cm}^{-2}$. Because of the high beam dilution, the regions inward of 0.5'' do not contribute to the observed SiC₂ emission. Assuming a mass-loss rate of $2 \times 10^{-5} M_\odot \text{ yr}^{-1}$ and an expansion velocity of 14.5 km s^{-1} , the total column density of H₂ in the 0.5–2'' region is $3 \times 10^{22} \text{ cm}^{-2}$, and the abundance of SiC₂ relative to H₂ is 2.9×10^{-7} .

The inner envelope abundance derived for SiC₂ (2.9×10^{-7} from the rotational diagram and 2×10^{-7} from the radiative transfer model) is in good agreement with the value computed under thermochemical equilibrium ($\sim 2 \times 10^{-7}$ from the photosphere up to $\sim 4 R_*$, using the code described in Tejero & Cernicharo 1991), and somewhat higher than the values calculated from non-equilibrium chemical modeling of the inner envelope ($10^{-9} - 10^{-8}$; Willacy & Cherchneff 1998). Previous studies based on millimeter-wave interferometric observations have derived values for the inner component of SiC₂ of 5×10^{-7} (Lucas et al., 1995) and $< 5 \times 10^{-8}$ (Gensheimer et al., 1995), in reasonable agreement with our derived values. Furthermore, these observational studies also find an enhancement of the SiC₂ abundance, up to $\sim 10^{-6}$ relative to H₂, in the outer envelope of IRC +10216, implying that additional formation routes must be at work in these outer regions. MacKay & Charnley (1999) studied the chemistry of silicon in IRC +10216 and were unable to find any reaction that could enhance the abundance of this species in the outer envelope. Our chemical model predicts such an abundance enhancement (see below).

To get a more reliable estimate of the abundance of SiC₂ in the inner regions and for insight into the peculiar chemistry of this species from the inner to the outer layers of the CSE, we carried out radiative transfer and chemical modeling calculations. We assumed a mass loss rate of $2 \times 10^{-5} M_\odot \text{ yr}^{-1}$, a stellar radius of $4 \times 10^{13} \text{ cm}$, a photospheric temperature of 2330 K, and a distance of 120 pc (see Agúndez 2009 and references therein). We assumed that the rotational levels of SiC₂ are thermalized. This approximation is adopted owing to the lack of information on the collision rate coefficients for high energy levels of SiC₂, and is

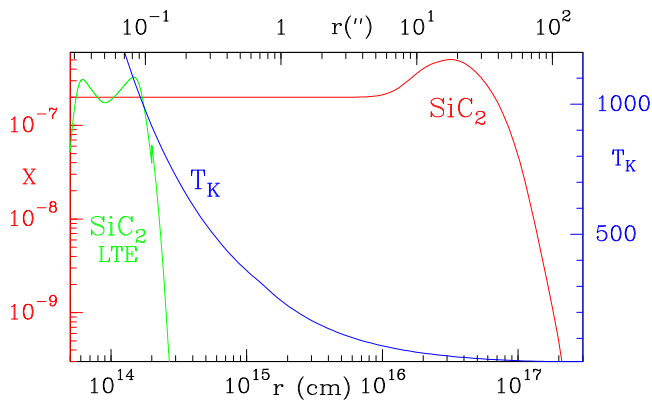


Fig. 3. Abundance of SiC₂, X , derived from the chemical model described in the text (red line) and in thermodynamical equilibrium (green line). The blue line shows the kinetic temperature, T_K , of the gas. The axis shows the distance to the star in cm (bottom) and the angular distance (top) as seen from the Earth ($d=120$ pc).

justified by the fact that the lines observed with HIFI are formed in the warm and dense inner regions of the CSE. Furthermore, IR pumping of the lines was not included in our model. We find that adopting an SiC₂ abundance of 2×10^{-7} relative to H₂ in the inner envelope reproduces the SiC₂ line profiles and intensities observed with HIFI reasonably well (see Fig. 4). The largest deviation between modeled and observed line profiles is 30% for the weakest lines. In good agreement with the abundance derived from the rotational diagram, we adopted an initial SiC₂ abundance of 2×10^{-7} at a radius of 10^{15} cm, and followed the chemical composition of the gas as it expands out to the outer layers of the envelope (see Fig. 3). We find that the SiC₂ abundance is slightly enhanced in the outer envelope up to a value of 5×10^{-7} (Fig. 3). Provided that the rapid reaction at low temperatures between Si and C₂H yields SiC₂ (Canosa et al., 2001), this reaction is the main source of this enhancement, along with the reaction between Si and C₂H, which is assumed to occur at a rate of 10^{-10} cm³ s⁻¹. The uncertainties on the reaction rates of the former reaction are, however, still large. The reaction of Si⁺ and C₂H also provides a formation route to SiC₂ through a sequence of ion-neutral reactions. The chemical model indicates that SiC₂ is finally photodissociated to form SiC, which is not detected in our HIFI spectral survey, although it has been observed before in the outer envelope layers (Cernicharo et al., 1989).

The present work confirms that SiC₂, together with SiS and SiO, is one of the major silicon carriers in the inner envelope of IRC +10216. SiC₂ is likely formed under thermochemical equilibrium conditions near the photosphere and it may also play an important role in silicon carbide dust formation in the ejecta. The full HIFI line survey of IRC +10216 will be presented in a series of forthcoming papers.

Acknowledgements. HIFI has been designed and built by a consortium of institutes and university departments from across Europe, Canada, and the United States (NASA) under the leadership of SRON, Netherlands Institute for Space Research, Groningen, The Netherlands, and with major contributions from Germany, France and the US. Consortium members are Canada: CSA, U. Waterloo; France: CESR, LAB, LERMA, IRAM; Germany: KOSMA, MPIfR, MPS; Ireland: NUI Maynooth; Italy: ASI, IFSI-INAF, Osservatorio Astrofisico di Arcetri-INAF; Netherlands: SRON, TUD; Poland: CAMK, CBK; Spain: Observatorio Astronómico Nacional (IGN), Centro de Astrobiología (INTA-CSIC); Sweden: Chalmers University of Technology - MC2, RSS & GARD, Onsala Space Observatory, Swedish National Space Board, Stockholm University - Stockholm Observatory; Switzerland: ETH Zurich, FHNW; USA: CalTech, JPL, NHSC. MG and EF acknowledge the support from the Centre

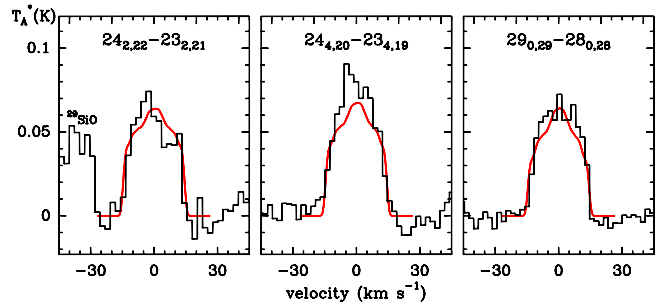


Fig. 4. Comparison between the line profiles of three rotational transitions of SiC₂ as observed with HIFI (black histograms) and as calculated with the radiative transfer model (red lines) using the abundance profile shown in red in Fig. 3.

National de Recherche Spatiale (CNES). JC, MA, JRG, JRP, CSC, and FD thank the Spanish MICINN for funding support under grants AYA2006-14876, AYA2009-07304, and CSD2009-00038. LD and EDB acknowledge financial support from the Fund for Scientific Research - Flanders (FWO). H.S.P.M. is grateful for support by the Bundesministerium für Bildung und Forschung (BMBF) administered through the Deutsches Zentrum für Luft- und Raumfahrt (DLR), whose support was aimed in particular at maintaining the CDMS.

References

- Agúndez, M., & Cernicharo, J., 2006, *ApJ*, 650, 374
 Agúndez, M. 2009, PhD Thesis, Universidad Autónoma de Madrid
 Bujarrabal, V., et al., 2010, this volume
 Canosa, A., Le Picard, S. D., Gougeon, S., et al. 2001, *J. Chem. Phys.*, 115, 6495
 Cernicharo, Kahane, C., J., Guélin, M., et al., 1986, *A&A*, 167, L9
 Cernicharo, J., & Guélin, M. 1987, *A&A*, 183, L10
 Cernicharo, J., Gottlieb, C.A., Guélin, M., et al., 1989, *ApJ*, 341, L25
 Cernicharo, J., Guélin, M., Kahane, C., et al., 1991, *A&A*, 246, 213
 Cernicharo, J., Barlow, M., González, E., et al., 1996a, *A&AS*, 315, L201
 Cernicharo, J., & Guélin, 1996b, *A&A*, 309, 127
 Cernicharo, J., 2004, *ApJ*, 608, L41
 Cernicharo, J., Guélin, M., & Kahane, C. 2000, *A&AS*, 142, 181
 Cernicharo, J., Guélin, M., Agúndez, M. et al., 2008, *ApJ*, 688, L83
 Cernicharo, J., Agúndez, M., Kahane, C., et al., 2010a, *ApJ*, in press
 Cernicharo, J., et al., 2010b, *A&A*, 518, L136
 Cernicharo, J., et al., 2010c, *A&A*, 518, L115
 Decin et al., 2010, *A&A*, 518, L143
 de Graauw T. et al. 2010, 518, L6
 Fonfría, J.P., Agúndez, M., Tercero, B., et al., *ApJ*, 646, L27
 Fonfría, J.P., Cernicharo, J., Richter, M.J., Lacy, J.H., 2008, *ApJ*, 673, 445
 Gensheimer, P.D., Likkell, L., Snyder, L.E., 1995, *ApJ*, 439, 445
 Gottlieb, C. A., Vrtilek, J. M., & Thaddeus, P. 1989, *ApJ*, 343, L29
 Griffin et al. 2010, *A&A*, 518, L3
 Guélin, M., Lucas, R., Cernicharo, J., 1993, *A&A*, 280, L19
 Guilloteau, S., Omont, A., Lucas, R., 1987, *A&A*, 170, L24
 He, J.H. et al., 2008, *ApJS*, 177, 275
 Herpin, F. & Cernicharo, J., 2001, *ApJ*, 530, L129
 Herpin, F., Goicoechea, J.R., Pardo, J.R., Cernicharo, J., 2002, *ApJ*, 577, 961
 Kemper, F., Stark, R., Justanont, K., de Koter, A., Tielens, A. G. G. M., Waters, L. B. F. M., Cami, J., & Dijkstra, C. 2003, *A&A*, 407, 609
 Lucas, R. & Cernicharo, J., 1989, *A&A*, 218, L20
 Lucas, R., Guélin, M., Kahane, C., et al., 1995, *Ap&SS*, 224, 293
 Lucas, R., 1997, *Ap&SS*, 251, 247
 MacKay, D.D.S., Charnley, S.B., 1999, *MNRAS*, 302, 793
 McCarthy, M.C., Gottlieb, C.A., Gupta, H., Thaddeus, P., 2006, *ApJ*, 652, L141
 Müller, H. S. P., Thorwirth, S., Roth, D. A., & Winnewisser, G. 2001, *A&A*, 370, L49
 Müller, H. S. P., Schlöder, F., Stutzki, J., & Winnewisser, G. 2005, *J. Mol. Struct.*, 742, 215
 Pardo, J.R. & Cernicharo, J., *ApJ*, 654, 978
 Patel, N.A., Young, K.H., Brüunken, S., et al., 2009, *ApJ*, 692, 1205
 Patel, N.A., Young, K.H., Brüunken, S., et al., 2009b, *ApJ*, 691, L55
 Pickett, H. M., Poynter, R. L., Cohen, E. A., et al. 1998, *J. Quant. Spectrosc. Radiat. Transfer*, 60, 883
 Pilbratt et al., 2010, *A&A*, 518, L1
 Poglitsch et al., 2010, *A&A*, 518, L2
 Roelfsema, P.R., et al., *A&A*, 2010, this volume

Schilke, P., Mehringer, D.M., Menten, K.M., 2000, ApJ, 528, L37
Schilke, P., Menten, K.M., 2003, ApJ, 583, 446
Suenram, R. D., Lovas, F. J., & Matsumura, K. 1989, ApJ, 342, L103
Thaddeus, P., Cummins, S.E., Linke, R.A., 1984, ApJ, 283, L45
Tejero, J. & Cernicharo, J. 1991, Instituto Geográfico Nacional, Madrid
Turner, B.E., 1987, A.&a., 183, L23
Willacy K., Cherchneff, I., 1998, A&A, 330, 676
Zelinger, Z., Amano, T., Ahrens, V., et al. 2003, J. Mol. Spectrosc., 220, 223

- ¹ Departamento de Astrofísica, Centro de Astrobiología, CSIC-INTA, Ctra. de Torrejón a Ajalvir km 4, Torrejón de Ardoz, 28850 Madrid, Spain
e-mail: jcernicharo@cab.inta-csic.es
- ² Astronomical Institute Anton Pannekoek, University of Amsterdam, Science Park XH, Amsterdam, The Netherlands
- ³ Instituut voor Sterrenkunde, Katholieke Universiteit Leuven, Celestijnenlaan 200D, 3001 Leuven, Belgium
- ⁴ LERMA and UMR 8112 du CNRS, Observatoire de Paris, 61 Av. de l'Observatoire, 75014 Paris, France
- ⁵ Leiden observatory, Leiden University, PO Box 9513, NL-2300 RA Leiden, The Netherlands
- ⁶ LUTH, Observatoire de Paris-Meudon, 5 Place Jules Janssen, 92190 Meudon, France
- ⁷ I. Physikalisches Institut, University of Cologne, Germany
- ⁸ Dept of Physics & Astronomy, University College London, Gower St, London WC1E 6BT, UK
- ⁹ Institute of Astronomy, ETH Zurich, 8093 Zurich, Switzerland
- ¹⁰ INAF - Istituto di Fisica dello Spazio Interplanetario, Area di Ricerca di Tor Vergata, via Fosso del Cavaliere 100, I-00133 Roma, Italy
- ¹¹ Department of Physics and Astronomy, University of Waterloo, Waterloo, ON Canada N2L 3G1
- ¹² Jet Propulsion Laboratory, 4800 Oak Grove Drive, MC 168-314, Pasadena, CA 91109 U.S.A.
- ¹³ European Space Astronomy Centre, ESA, P.O. Box 78, E-28691 Villanueva de la Cañada, Madrid, Spain
- ¹⁴ Astronomical Institute, Utrecht University, Princetonplein 5, 3584 CC, Utrecht, The Netherlands
- ¹⁵ Department of Radio and Space Science, Chalmers University of Technology, Onsala Space Observatory, 439 92 Onsala, Sweden
- ¹⁶ University of Massachusetts, Astronomy Dept., 710 N. Pleasant St., LGRT-619E, Amherst, MA 01003-9305 U.S.A.
- ¹⁷ SRON Netherlands Institute for Space Research, Landleven 12, 9747 AD Groningen, The Netherlands

Appendix A: SiC₂ Spectroscopy

Silacyclopropynylidene, SiC₂, is a triangular molecule with a dipole moment of 2.393 (6) D (Suenram et al., 1989) along the *a*-axis. *R*-branch transitions with $\Delta K_a = 0$ are the strongest ones. The molecule is fairly asymmetric, $\kappa = (2B - A - C)/(A - C) = -0.7117$; therefore, *Q*-branch transitions with $\Delta K_a = 0$ and transitions with $\Delta K_a = \pm 2$ also have considerable intensities. Measurements of such transitions, even at low frequencies, may improve predictions of $\Delta K_a = 0$ *R*-branch transitions at higher frequencies. SiC₂ has a low-lying asymmetric bending mode ν_3 , this may lead to non-negligible changes in the dipole moment with K_a . Only transitions with even K_a are allowed because of the spin statistics associated with the two equivalent C nuclei. The rotational spectrum of the main isotopic species of SiC₂ has been studied to some extent. Thaddeus et al. (1984) reported the first detection of this species towards IRC +10216 based on laboratory measurements of several rotational lines. Cernicharo et al. (1986) reported the detection of ²⁹SiC₂ and ³⁰SiC₂ based on astronomical observations. Suenram et al. (1989) recorded the $J = 1 - 0$ transitions of the three silicon isotopologs of SiC₂. The detection of Si¹³CC in space was reported by Cernicharo et al. (1991) based on astronomical and laboratory observations. In the same paper they reported tens of SiC₂, ²⁹SiC₂, ³⁰SiC₂, and Si¹³CC lines detected in IRC +10216 with frequency accuracies ranging between 0.2 and 1.0 MHz. At about the same time, Gottlieb et al. (1989) reported 34 transitions recorded between 90 and 370 GHz. Even though the number of parameters (15) was large, the data were only reproduced to within four times the quoted uncertainties. He et al. (2008) found that the data could be reproduced almost within the reported uncertainties if, instead of Watson's *A*-, the *S*-reduction was used with two more parameters plus an additional one that was estimated. To obtain a balanced fit, the uncertainties from Gottlieb et al. (1989) were multiplied by 1.5. The resulting fit was the basis of the CDMS² catalog entry (Müller et al., 2001, 2005).

The issue of the uncertainties reported for the laboratory lines of Gottlieb et al. and their choice of parameters to fit the data has already been discussed in the He et al. (2008) paper. There it is pointed out that, despite a large number of spectroscopic parameters used in the fit, the experimental data was only reproduced within four times the reported uncertainties. He et al. were able to reproduce the data much better by switching from the *A* reduction (which was providing negative energies for $J > 25$ using the Gottlieb et al. parameters) to the *S* reduction and by increasing the number of parameters somewhat. However, they were only able to reproduce the laboratory data within 1.5 times the experimental uncertainties. This finding suggests that the experimental error estimates may have been too optimistic, at least as long as no model is available to reproduce the experimental data better than the model of He et al. Moreover, the increase in experimental uncertainties by 50% may well be too little because a rather large set of spectroscopic parameters was needed to fit a rather small set of experimental lines of this admittedly non rigid molecule. As discussed below, we found in the present investigation that the modified uncertainties by He et al. are appropriate for our present, more larger data set. The strong transitions are predicted quite well up to about 500 GHz, but the quality of the prediction deteriorates rapidly at higher frequencies, as it turned out, in particular for lower values of K_a . Therefore, the SiC₂ transition frequencies from the present HIFI observations were sub-

jected to a combined fit with the laboratory data. Table A.2 compares the present parameters with those from He et al. (2008). All parameters were improved, especially the ones that depend particularly on J . Even though the parameter L_J was newly introduced, the uncertainty of H_J also decreased. In most cases, the parameter values differ only slightly from the previous ones, validating the previous model. Some changes outside the uncertainties are likely caused by including L_J in the fit. He et al. (2008) have already found that only slight modifications of the parameter values are required to fit isotopic data from their, and previous astronomical (Cernicharo et al., 1991) and laboratory data (Suenram et al., 1989). The SiC₂ lines detected in the HIFI 1b survey, their uncertainties, and residuals are listed in Table A.1.

² We made use of the CDMS (Müller et al., 2001, 2005, <http://www.cdms.de>) and JPL (Pickett et al., 1998, <http://spec.jpl.nasa.gov>) molecular data bases in this work.

Table A.1. Observed SiC₂ transitions J^u_{Ka,Kc}-J^l_{Ka,Kc}.

Transition J ^u _{Ka,Kc} -J ^l _{Ka,Kc}	Obs. Freq. (MHz)	o-c (MHz)	S	E _l /k (K)	I _v (K km/s)
24 _{2,22} -23 _{2,21}	557109.0(1.5)	1.43	23.5	328.2	1.42(3)
24 _{12,13} -23 _{12,12}	557600.0(1.5)	0.27	18.0	589.7	0.32(3)
24 _{12,12} -23 _{12,11}	557600.0(1.5)	0.27	18.0	589.7	0.32(3)
24 _{10,15} -23 _{10,14}	562069.0(5.0)	-1.09	19.9	505.2	0.45(11)
24 _{10,14} -23 _{10,13}	562069.0(5.0)	-1.09	19.9	505.2	0.45(11)
24 _{8,17} -23 _{8,16}	566903.0(6.0)	7.29	21.4	436.6	0.74(5)
24 _{8,16} -23 _{8,15}	566912.0(6.0)	9.90	21.4	436.6	0.74(5)
24 _{4,21} -23 _{4,20}	568464.0(1.5)	-0.55	23.3	346.2	1.25(2)
25 _{16,10} -24 _{16,9}	571113.0(6.0)	2.06	14.8	832.7	0.14(3)
25 _{16,9} -24 _{16,8}	571113.0(6.0)	2.06	14.8	832.7	0.14(3)
23 _{4,19} -22 _{4,18}	571141.0(1.5)	2.43	22.4	324.6	1.46(2)
24 _{6,19} -23 _{6,18}	572966.0(1.5)	2.02	22.5	384.1	0.90(2)
27 _{0,27} -26 _{0,26}	573938.0(1.5)	-0.07	26.9	364.7	1.48(2)
26 _{2,25} -25 _{2,24}	574425.0(1.5)	1.53	25.7	361.9	1.27(2)
24 _{6,18} -23 _{6,17}	574577.0(1.5)	3.70	22.5	384.2	1.02(2)
25 _{14,12} -24 _{14,11}	576122.0(6.0)	-3.08	17.2	716.6	0.13(3)
25 _{14,11} -24 _{14,10}	576122.0(6.0)	-3.08	17.2	716.6	0.13(3)
25 _{2,23} -24 _{2,22}	577234.0(1.5)	0.69	24.5	355.0	1.39(2)
25 _{12,14} -24 _{12,13}	580951.0(1.5)	0.97	19.3	616.4	0.31(2)
25 _{12,13} -24 _{12,12}	580951.0(1.5)	0.97	19.3	616.4	0.31(2)
25 _{10,16} -24 _{10,15}	585735.0(1.5)	-0.44	21.0	532.2	0.44(2)
25 _{10,15} -24 _{10,14}	585735.0(1.5)	-0.44	21.0	532.2	0.44(2)
25 _{8,18} -24 _{8,17}	590972.0(2.5)	0.41	22.5	463.8	0.66(2)
25 _{4,22} -24 _{4,21}	590814.0(1.5)	-1.58	24.3	373.5	1.09(1)
25 _{8,17} -24 _{8,16}	590990.0(2.5)	3.89	22.5	463.8	0.66(2)
28 _{0,28} -27 _{0,27}	594745.0(1.5)	-0.57	27.9	392.2	1.46(3)
27 _{2,26} -26 _{2,25}	595235.0(1.5)	2.63	26.7	389.4	1.43(3)
24 _{4,20} -23 _{4,19}	596691.0(1.5)	0.51	23.4	352.0	1.76(2)
25 _{6,20} -24 _{6,19}	597462.0(5.0)	-0.07	23.6	411.6	0.86(4)
26 _{2,24} -25 _{2,23}	597477.0(2.5)	-0.93	25.5	382.7	1.10(4)
26 _{14,13} -25 _{14,12}	599184.0(4.0)	-9.03	18.5	744.2	0.14(2)
26 _{14,12} -25 _{14,11}	599184.0(4.0)	-9.03	18.5	744.2	0.14(2)
25 _{6,19} -24 _{6,18}	599914.0(1.5)	0.11	23.6	411.8	0.85(2)
26 _{12,14} -25 _{12,13}	604324.0(6.0)	7.38	20.5	644.3	0.38(3)
26 _{12,15} -25 _{12,14}	604324.0(6.0)	7.38	20.5	644.3	0.38(3)
26 _{10,16} -25 _{10,15}	609433.0(1.5)	-0.94	22.2	560.3	0.47(1)
26 _{10,17} -25 _{10,16}	609433.0(1.5)	-0.94	22.2	560.3	0.47(1)
26 _{4,23} -25 _{4,22}	612914.0(1.5)	-0.82	25.3	401.8	1.09(1)
26 _{8,19} -25 _{8,18}	615115.0(4.0)	-0.21	23.6	492.2	0.78(2)
26 _{8,18} -25 _{8,17}	615139.0(4.0)	2.45	23.6	492.2	0.70(2)
27 _{16,12} -26 _{16,11}	616666.0(6.0)	-1.46	17.6	888.7	0.06(1)
27 _{16,11} -26 _{16,10}	616666.0(6.0)	5.55	17.6	888.7	0.06(1)
29 _{0,29} -28 _{0,28}	615547.0(1.5)	5.55	28.9	420.8	1.55(2)
27 _{2,25} -26 _{2,24}	617833.0(1.5)	0.71	26.5	411.3	1.15(2)
25 _{4,21} -24 _{4,20}	621588.0(1.5)	-1.38	24.5	380.6	1.36(2)
26 _{6,21} -25 _{6,20}	621960.0(1.5)	0.96	24.7	440.3	0.91(2)
27 _{14,14} -26 _{14,13}	622264.0(6.0)	-1.00	19.8	773.0	0.11(1)
27 _{14,13} -26 _{14,12}	622264.0(6.0)	-1.00	19.8	773.0	0.11(1)
26 _{6,20} -25 _{6,19}	625591.0(1.5)	-1.43	24.7	440.6	1.06(2)
27 _{12,16} -26 _{12,15}	627699.0(1.5)	-0.23	21.7	673.3	0.34(1)
27 _{12,15} -26 _{12,14}	627699.0(1.5)	-0.23	21.7	673.3	0.34(1)
27 _{10,17} -26 _{10,16}	633168.0(1.5)	-0.26	23.3	589.6	0.45(2)
27 _{10,18} -26 _{10,17}	633168.0(1.5)	-0.26	23.3	589.6	0.45(2)
27 _{4,24} -26 _{4,23}	634776.0(1.5)	-2.96	26.3	431.2	1.15(3)
30 _{0,30} -29 _{0,29}	636346.0(1.5)	0.01	29.9	450.3	1.25(4)

Notes: The first column lists the quantum numbers of the transitions. *o - c* corresponds to observed minus calculated frequencies. *S* is the line strength and *E_l* is the energy of the lower level of the transition. $I_v = \int T_A dv$ is the integrated intensity. Values in parentheses are uncertainties in units of the last digits

Table A.2. Spectroscopic parameters^a (MHz) for SiC₂ obtained in the present investigation compared to a previous study.

Parameter	This work	He et al. 2008
$A - (B + C)/2$	40674.000 (81)	40674.191 (100)
$(B + C)/2$	11800.11932 (84)	11800.11861 (99)
$(B - C)/4$	678.41182 (76)	678.41301 (130)
D_K	-1.3429 (185)	-1.2880 (227)
D_{JK}	1.624141 (59)	1.624219 (88)
$D_J \times 10^3$	-1.1651 (80)	-1.1845 (115)
$d_1 \times 10^3$	-2.4371 (53)	-2.4392 (111)
$d_2 \times 10^3$	-7.1766 (30)	-7.2002 (80)
$H_{KJ} \times 10^6$	669.68 (104)	670.39 (151)
$H_{JK} \times 10^6$	-138.26 (12)	-138.66 (39)
$H_J \times 10^6$	0.9810 (187)	1.0079 (201)
$h_1 \times 10^9$	-193.0 (101)	-180.2 (247)
$h_2 \times 10^9$	-578.1 (84)	-513.3 (301)
$h_3 \times 10^9$	185.8 (67)	157.0 (93)
$L_{KKJ} \times 10^9$	-135.4 (69)	-138.5 (80)
$L_{JK} \times 10^9$	14.68 (175)	14.34 (266)
$L_{JJK} \times 10^9$	-12.11 (28)	-11.06 (78)
$L_J \times 10^{12}$	138.9 (166)	-
$P_{KKKJ} \times 10^{12}$	20. ^b	20. ^b

^a Watson's *S*-reduction was used in the representation *I'*. Numbers in parentheses are 1 σ uncertainties in units of the least significant figures.

^b Kept fixed to estimated value.